A Carboxylate-Bridged Non-Heme Diiron Dinitrosyl Complex

Andrew L. Feig, Maria T. Bautista, and Stephen J. Lippard*

Department of Chemistry, Massachusetts Institute of Technology, Cambridge, Massachusetts 02139

Received May 16, 1996[⊗]

The reaction of nitric oxide with the carboxylate-bridged diiron(II) complex $[Fe_2(Et\text{-}HPTB)(O_2CPh)](BF_4)_2$ (**1a**) afforded the dinitrosyl adduct, $[Fe_2(NO)_2(Et\text{-}HPTB)(O_2CPh)](BF_4)_2$ (**1b**), where Et-HPTB = *N*,*N*,*N*′,*N*′-tetrakis-(*N*-ethyl-2-benzimidazolylmethyl)-2-hydroxy-1,3-diaminopropane, in 69% yield. Compound **1b** further reacts with dioxygen to form the bis(nitrato) complex, $[Fe_2(Et\text{-}HPTB)(NO_3)_2(OH)](BF_4)_2$ (**1c**). The structure of **1b** was determined by X-ray crystallography (triclinic, $P\bar{1}$, $a = 13.5765(8)$ Å, $b = 15.4088(10)$ Å, $c = 16.2145(10)$ Å, $\alpha = 73.656(1)°$, $\beta = 73.546(1)°$, $\gamma = 73.499(1)°$, $V = 3043.8(7)$ Å^3, $T = -80$ °C, $Z = 2$, and $R = 0.085$ and $R_w = 0.095$ for 5644 independent reflections with $I > 3\sigma(I)$). The two nitrosyl units are equivalent with an average Fe−N−O angle of 167.4 ± 0.8°. Spectroscopic characterization of solid **1b** revealed an NO stretch at 1785 cm^{-1} in the infrared and Mössbauer parameters of $\delta = 0.67$ mm s^{-1} and $\Delta E_Q = 1.44$ mm s^{-1} at 4.2 K. These data are comparable to those for other {FeNO}^{7} systems. An $S = {}^3/_2$ spin state was assigned from magnetic susceptibility studies to the two individual {FeNO} centers, each of which has a nitrosyl ligand antiferromagnetically coupled to iron. A least-squares fit of the χ vs temperature plots to a theoretical model yielded an exchange coupling constant J of −23 cm^{-1}, where $H = -2J\mathbf{S}_1\cdot\mathbf{S}_2$, indicating that the two $S = {}^3/_2$ centers are antiferromagnetically coupled to one another. An extended Hückel calculation on a model complex, $[Fe_2(NO)_2(NH_3)_6(O_2CH)(OH)]^{2+}$, revealed that the magnitudes of Fe−N−O angles are dictated by π-bonding interactions between the Fe d_{xz} and NO π* orbitals.

Introduction

Many important biological processes are promoted by non-heme iron proteins where the activity is initiated by coordination of O_2 to the metal core.[1] The reaction of dioxygen with a single metal center produces a highly reactive superoxo intermediate that is difficult to isolate and characterize. Owing to similarities in the manner by which O_2 and NO interact with transition metal centers, insight into the O_2-binding process can be gained by preparation of the corresponding nitrosyl adducts.[2] An additional advantage of synthesizing the NO adducts is their greater stability compared to that of the dioxygen analogs, since reaction of the monoradical NO with a paramagnetic transition metal center results in a closed-shell configuration for the nitrosyl ligand. Examples of mononuclear non-heme iron proteins that bind NO include protocatechuate-4,5-dioxygenase,[3] putidamonooxin,[4,5] soybean lipoxygenase,[6] and isopenicillin N synthase.[7] The reactivity of these active sites toward NO is also modeled by several mononuclear iron(II) complexes.[8−11] There are two reports of non-heme diiron proteins that bind NO, namely hemerythrin (Hr) and ribonucleotide reductase (R2).[12,13]

Transition metal nitrosyl complexes have attracted a considerable amount of experimental and theoretical interest in their own right.[14−17] Nitrosyl ligands can adopt a variety of metal-binding configurations, as manifest by M−N−O angles ranging between 120 and 180°. Determining the metal oxidation state in these nitrosyl complexes has proved to be complicated because of the very small energy difference between transition metal d and NO π* orbitals, which makes it difficult to define the character of the donor and acceptor levels. To circumvent this problem, the notation {MNO}^{x} has been adopted, where x represents the sum of the electrons in the metal d and NO π* orbitals.[14]

Although dinuclear iron nitrosyl complexes are known, they contain phosphine,[18] thiolate,[19,20] or sulfide[21,22] ligands. Surprisingly, no synthetic carboxylate-bridged non-heme diiron analogs of Hr or R2 have been reported that mimic the NO binding ability of these proteins. We therefore investigated the reaction of the diferrous complex $[Fe_2(Et\text{-}HPTB)(O_2CPh)](BF_4)_2$ (**1a**) (Et-HPTB = *N*,*N*,*N*′,*N*′-tetrakis(*N*-ethyl-2-benzimidazolylmethyl)-1,3-diaminopropane)[23] with nitric oxide. A major

[⊗] Abstract published in *Advance ACS Abstracts,* October 1, 1996.

(1) Feig, A. L.; Lippard, S. J. *Chem. Rev.* **1994**, *94*, 759.
(2) Richter-Addo, G. B.; Legzdins, P. *Metal Nitrosyls*; Oxford University Press: New York, 1992; p 256.
(3) Arciero, D. M.; Lipscomb, J. D.; Huynh, B. H.; Kent, T. A.; Münck, E. *J. Biol. Chem.* **1983**, *258*, 14981.
(4) Bill, E.; Bernhardt, F.-H.; Trautwein, A. X.; Winkler, H. *Eur. J. Biochem.* **1985**, *147*, 177.
(5) Twilfer, H.; Bernhardt, F.-H.; Gersonde, K. *Eur. J. Biochem.* **1985**, *147*, 171.
(6) Nelson, M. J. *J. Biol. Chem.* **1987**, *262*, 12137.
(7) Chen, V. J.; Orville, A. M.; Harpel, M. R.; Frolik, C. A.; Surerus, K. K.; Münck, E.; Lipscomb, J. D. *J. Biol. Chem.* **1989**, *264*, 21677.
(8) Wells, F. V.; McCann, S. W.; Wickman, H. H.; Kessel, S. L.; Hendrickson, D. N.; Feltham, R. D. *Inorg. Chem.* **1982**, *21*, 2306.
(9) Farrar, J.; Grinter, R.; Pountney, D. L.; Thomson, A. J. *J. Chem. Soc., Dalton Trans.* **1993**, 2703.
(10) Zhang, Y.; Pavlosky, M. A.; Brown, C. A.; Westre, T. E.; Hedman, B.; Hodgson, K. O.; Solomon, E. I. *J. Am. Chem. Soc.* **1992**, *114*, 9189.
(11) Brown, C. A.; Pavlosky, M. A.; Westre, T. E.; Zhang, Y.; Hedman, B.; Hodgson, K. O.; Solomon, E. I. *J. Am. Chem. Soc.* **1995**, *117*, 715.
(12) Nocek, J. M.; Kurtz, D. M., Jr.; Sage, J. T.; Xia, Y.-M.; Debrunner, P.; Shiemke, A. K.; Sanders-Loehr, J.; Loehr, T. M. *Biochemistry* **1988**, *27*, 1014.
(13) Haskin, C. J.; Ravi, N.; Lynch, J. B.; Münck, E.; Que, L., Jr. *Biochemistry* **1995**, *34*, 11090.
(14) Enemark, J. H.; Feltham, R. D. *Coord. Chem. Rev.* **1974**, *13*, 339.
(15) Mingos, D. M. P.; Sherman, D. J. *Adv. Inorg. Chem.* **1989**, *34*, 293.
(16) McCleverty, J. A. *Chem. Rev.* **1979**, *79*, 53.
(17) Hoffmann, R.; Chen, M. M. L.; Elian, M.; Rossi, A. R.; Mingos, D. M. P. *Inorg. Chem.* **1974**, *13*, 2666.
(18) Guillaume, P.; Wah, H. L. K.; Postel, M. *Inorg. Chem.* **1991**, *30*, 1828.
(19) Butler, A. R.; Glidewell, C.; Hyde, A. R.; McGinnis, J.; Seymour, J. E. *Polyhedron* **1983**, *2*, 1045.
(20) Glidewell, C.; Harman, M. E.; Hursthouse, M. B.; Johnson, I. L.; Motevalli, M. *J. Chem. Res. Synop.* **1988**, *7*, 212.
(21) Rauchfuss, T. B.; Weatherill, T. D. *Inorg. Chem.* **1982**, *21*, 827.
(22) Glidewell, C.; Hyde, A. R.; McKechnie, J. S.; Pogorzelec, P. J. *J. Chem. Educ.* **1985**, *62*, 534.

S0020-1669(96)00552-6 CCC: $12.00 © 1996 American Chemical Society

product is the dinitrosyl adduct, $[Fe_2(Et\text{-}HPTB)(O_2CPh)(NO)_2](BF_4)_2$ (**1b**), and we report here its characterization by single-crystal X-ray diffraction, magnetic susceptibility, Mössbauer, optical, and infrared spectroscopic, and extended Hückel theoretical techniques. In **1b**, the oxidation states of the iron−nitrosyl units can be assigned formally as Fe(II)−NO or Fe(III)−NO^-; we write the centers as $\{FeNO\}^7$ to account for the total of iron d electrons and NO π^* electrons.

Experimental Section

General Considerations. Anaerobic work was carried out in a nitrogen-filled glovebox or by using standard Schlenk techniques. Solvents used in the synthetic and catalytic reactions were dried and distilled by standard procedures. Nitric oxide (99+%) was purchased from Matheson and extensively purified as described.[24] The purification system was purged with argon prior to the initiation of an experiment to ensure removal of any adventitious O_2. The stability of the nitrosyl adduct was diminished if the NO purification step was omitted. The diiron(II) precursor, $[Fe_2(Et\text{-}HPTB)(O_2CPh)](BF_4)_2$ (**1a**), was prepared as described previously and recrystallized from acetonitrile/Et_2O.[23]

Instrumentation. Optical spectra were recorded on a HP 8452 diode array spectrophotometer. A Bio-Rad FTS7 FTIR spectrometer was used to measure vibrational spectra of KBr pellets.

Synthesis of $[Fe_2(Et\text{-}HPTB)(O_2CPh)(NO)_2](BF_4)_2$ (1b). The reaction of excess NO gas with **1a** (0.30 g, 0.27 mmol) in acetonitrile, propionitrile, or chloroform solutions resulted in an immediate color change from yellow to dark brown-green. This solution was layered with NO-saturated diethyl ether via cannula and was allowed to stand for several days, yielding dark green needles of **1b** (0.22 g, 69% yield). To grow X-ray diffraction quality crystals, septum-sealed crystallization vials containing acetonitrile solutions of **1a** were placed in a central container surrounded by diethyl ether. The N_2 atmosphere within the vial was replaced with NO by rapid sparging. Upon standing overnight, dark green crystals of **1b** formed. Anal. Calcd for $C_{50}H_{54}N_{12}O_5B_2F_8Fe_2$: C, 50.54; H, 4.58; N, 14.14. Found: C, 51.15; H, 4.61; N, 13.40. IR (cm^{-1}, KBr pellet): 1785 (m, ν_{NO}), 1617 (m), 1594 (m), 1550 (m), 1541 (sh), 1494 (s), 1456 (s), 1400 (sh), 1385 (m), 1332 (m), 1294 (m), 1278 (m), 1237 (m), 1237 (w), 1167 (w), 1057 (vs), 979 (m), 894 (m), 746 (s), 722 (m), 688 (w), 675 (m), 521 (m), 433 (w).

Synthesis of $[Fe_2(Et\text{-}HPTB)(OH)(NO_3)_2](BF_4)_2\cdot 0.5Et_2O\cdot 2H_2O$ (1c). Nitric oxide was bubbled into a 25 mL acetonitrile solution of **1a** (0.050 g, 0.044 mmol). Dioxygen was added to the resulting brown-green solution of **1b** to produce a red-orange color change. The product of this reaction, $[Fe_2(Et\text{-}HPTB)(OH)(NO_3)_2](BF_4)_2\cdot 0.5Et_2O\cdot 2H_2O$ (**1c**), was obtained in crystalline form by vapor diffusion of Et_2O into acetonitrile solutions of the complex (0.043 g, 80% yield). Compound **1c** is an exact analog of a complex reported having the HPTB ligand, which lacks the *N*-ethyl groups.[25] A crystal structure analysis of **1c** established its stoichiometry but displayed the same disorder problems previously noted for the related HPTB compound.[25,26] Crystal data: orthorhombic, $a = 15.037(1)$ Å, $b = 19.746(2)$ Å, $c = 21.038(3)$ Å, $V = 6247(1)$ Å^3. IR (cm^{-1}, KBr pellet): 1616 (w br, ν_{NO_2} asym), 1517 (m sh), 1496 (s), 1456 (s), 1384 (s), 1331 (m), 1294 (s), 1281 (s, ν_{NO_2} sym), 1237 (w), 1154 (w sh), 1125 (m sh), 1083 (s), 1063 (s br), 1016 (m sh), 978 (m), 953 (w), 931 (m), 908 (w), 893 (w), 854 (vw), 834 (vw), 805 (vw), 751 (s), 685 (m), 654 (vw), 625 (w), 578 (w), 542 (w), 522 (m), 457 (vw), 436 (w). Anal. Calcd for $C_{45}H_{59}N_{12}O_{10.5}Fe_2B_2F_8$: C, 44.25; H, 4.87; N, 13.76. Found: C, 44.27; H, 4.56; N, 13.78.

Collection and Reduction of X-ray Data. A single crystal was coated with Paratone-N oil (Exxon), attached to a quartz fiber, and transferred to a Siemens CCD X-ray diffraction system controlled by a pentium-based PC running the SMART software package.[27] The crystal was mounted on the three-circle goniometer with χ fixed at +54.79° and was rapidly cooled to −80 °C with a Siemens LT-2A nitrogen cryostat, calibrated with a copper−constantan thermocouple. The diffracted graphite-monochromated Mo Kα radiation ($\lambda = 0.710\ 73$ Å) was detected on a phosphor screen held at a distance of 6.0 cm from the crystal operating at −54 °C. A detector array of 512 × 512 pixels, with a pixel size of approximately 120 μm, was employed for data collection. The detector centroid and crystal-to-detector distance were calibrated from a least-squares analysis of the unit cell parameters of a carefully centered ylide test crystal. After the crystal of **1b** had been carefully optically centered within the X-ray beam, a series of 20 data frames measured at 0.3° increments of ω were collected with three different 2θ and ϕ values to assess the overall crystal quality and to calculate a preliminary unit cell. In order to correct for high-energy background events in the images, data frames were collected as the sum of two 5-s exposures and noncorrelating events were eliminated. A correction for the background detector current was also applied to the frames, and a small offset was added to all of the individual pixel values to prevent any statistical bias induced by truncating negative values to zero. The measured intensities of individual reflections were plotted at 0.3° intervals of ω, and the average peak width at baseline was less than 1.5°. A total of 63 reflections with $I > 10\sigma(I)$ were selected from the data frames and utilized to calculate a preliminary unit cell. For the collection of the intensity data, the detector was positioned at a 2θ value of −25° and the intensity images were measured at 0.3° intervals of ω for a duration of 10 s each. The data frames were collected in three distinct shells which, when combined, measured more than 1.3 hemispheres of intensity data with a maximum 2θ value of 46.5°. For the first shell, the crystal was positioned at $\phi = 0°$ and $\omega = -26°$ and a set of 606 frames was collected. A series of 435 frames was collected in the second shell with a starting position of $\phi = 88°$ and $\omega = -21.0°$. The crystal was then moved to a position of $\phi = 180°$ and $\omega = -23.00°$ to measure the 230 frames required for the third shell. The initial 50 frames of the first data shell were recollected at the end of data collection to correct for any crystal decay, but none was observed.

Immediately after collection, the raw data frames were transferred to a Silicon Graphics Indy workstation for integration by the SAINT program package.[28] An initial background and spot shape measurement were made, and these parameters, as well as the orientation matrix, were continuously updated during frame integration. The background frame information was updated according to eq 1, where B' is the update

$$B' = (7B + C)/8 \tag{1}$$

pixel value, B is the background pixel value before updating, and C is the pixel value in the current frame. The integration was also corrected for spatial distortions induced by the detector. In addition, pixels that reside outside of the detector active area or behind the beam stop were masked during frame integration. The integrated intensities for the three shells of data were merged to one reflection file. The data file was filtered to reject outlier reflections. The rejection of a reflection was based on the disagreement between the intensity of the reflection and the average intensity of the symmetry equivalents to which the reflection belongs. In the case of strong reflections ($I > 99\ \sigma(I)$) which contained only two equivalents, the larger of the two equivalents was retained. A total of 70 reflections, corresponding to 0.88% of the data, were excluded from the final reflection file for compound **1b**.

The structure was solved by direct methods by using SIR-92[29] and was refined by full-matrix least-squares and Fourier techniques with the program TEXSAN.[30] All non-hydrogen atoms were refined anisotropically. Hydrogen atoms were assigned idealized locations and were given a thermal parameter equivalent to 1.2 times the thermal parameter of the carbon atom to which it was attached. Final refinement yielded the residuals given in Table 1.

Magnetic Susceptibility Measurements. The magnetic susceptibility of a polycrystalline sample of **1b** (60 mg) was measured by using

(23) Dong, Y.; Ménage, S.; Brennan, B. A.; Elgren, T. E.; Jang, H. G.; Pearce, L. L.; Que, L., Jr. *J. Am. Chem. Soc.* **1993**, *115*, 1851.
(24) Ruggiero, C. E.; Carrier, S. M.; Antholine, W. E.; Whittaker, J. W.; Cramer, C. J.; Tolman, W. B. *J. Am. Chem. Soc.* **1993**, *115*, 11285.
(25) Brennan, B. A.; Chen, Q.; Juarez-Garcia, C.; True, A. E.; O'Connor, C. J.; Que, L., Jr. *Inorg. Chem.* **1991**, *30*, 1937.
(26) Feig, A. L.; Lippard, S. J. Unpublished results.
(27) *SMART: Version 4.0*; Siemens Industrial Automation, Inc.: Madison, WI, 1994.
(28) *SAINT: Version 4.0*; Siemens Industrial Automation, Inc.: Madison, WI, 1995.
(29) Burla, M. C.; Camalli, M.; Cascarano, G.; Giacovazzo, C.; Polidori, G.; Spagna, R.; Viterbo, D. *J. Appl. Crystallogr.* **1989**, *22*, 389.
(30) *TEXSAN*: *Single Crystal Structure Analysis Software, Version 1.6*; Molecular Structure Corp.: The Woodlands, TX, 1993.

Table 1. X-ray Crystallographic Information for $[Fe_2(Et\text{-}HPTB)(O_2CPh)_2(NO)_2](BF_4)_2 \cdot 3MeCN$ (**1b**·3MeCN).

formula	$Fe_2C_{56}H_{63}B_2F_8O_5N_{15}$
mol wt	1311.5
a (Å)	13.5765(8)
b (Å)	15.4088(10)
c (Å)	16.2145(10)
α (deg)	73.656(1)
β (deg)	73.546(1)
γ (deg)	73.499(1)
V (Å^3)	3043.8(7)
T (°C)	−80
Z	2
radiation, λ (Å)	Mo Kα, $\lambda = 0.71073$ Å
ρ_{calc} (g/cm^3)	1.43
space group	$P\bar{1}$
2θ limits (deg)	46.5
μ (cm^{-1})	5.52
tot. data	8052
unique data[a]	5644
no. of params	749
R[b]	0.085
R_w	0.095

[a] Observation criterion $I > 3\sigma(I)$. [b] $R = \Sigma||F_o| - |F_c||/\Sigma|F_o|$, $R_w = [\Sigma w(|F_o| - |F_c|)^2/\Sigma w|F_o|^2]^{1/2}$, where $w = 1/\sigma^2(F_o)$.[44]

a Quantum Design SQUID susceptometer. The sample was loaded anaerobically into a gel capsule and suspended in a plastic straw. A background correction for the empty capsule and straw was applied to the data, which were also corrected for underlying diamagnetism of -5.08×10^{-4} emu mol^{-1} as calculated from Pascal's constants.[31] A total of 40 data points were collected in the temperature range of 4.3 to 300 K at 5000 G.

Mössbauer Spectroscopic Measurement. A Mössbauer spectrum was recorded on 70 mg of polycrystalline **1b** at 4.2 K. The source was ^{57}Co in a Rh matrix maintained at 300 K. Isomer shifts were referenced to iron metal at 300 K.

Theoretical Calculations. Extended Hückel calculations were performed by using CACAO,[32] which also produced the Walsh diagrams (for seven points). To simplify the calculation, the theoretical complex, $[Fe_2(OH)(O_2CH)(NH_3)_6(NO)_2]^{2+}$ was analyzed.

Results

Description of the Structure. The dinitrosyl adduct, $[Fe_2(Et\text{-}HPTB)(O_2CPh)(NO)_2](BF_4)_2$ (**1b**), crystallized in the triclinic space group $P\bar{1}$. An ORTEP drawing of the cation is shown in Figure 1. A table of positional parameters is provided in Table 2, and selected interatomic distances and angles are listed in Tables 3 and 4. The two halves of the molecule are related by a noncrystallographic mirror plane passing through O(1), C(2), C(44), C(45), and C(48) (Figure 1), with the geometry at each iron atom being best described as distorted octahedral. The benzimidazole substituents of Et-HPTB ligand are syn to one another across the pseudo-mirror plane, a feature also observed in a tetranuclear Fe(III) complex of the Et-HPTB ligand.[33] The alternative, anti, geometry, was observed in the bis(nitrato)-diiron(III) complexes of the related HPTB and HPTP ligands (HPTP = *N*,*N*,*N*′,*N*′-tetrakis(2-pyridylmethyl)-1,3-diaminopropane).[25,34] The factors that dictate the favored coordination mode are presently unclear. The Fe−O−Fe angle of 117.7° in **1b** is in the range of values found in other diiron or dimanganese complexes of ligands having both μ-alkoxo and μ-carboxylato coordination.[23,33,35,36] The most substantial distortions from

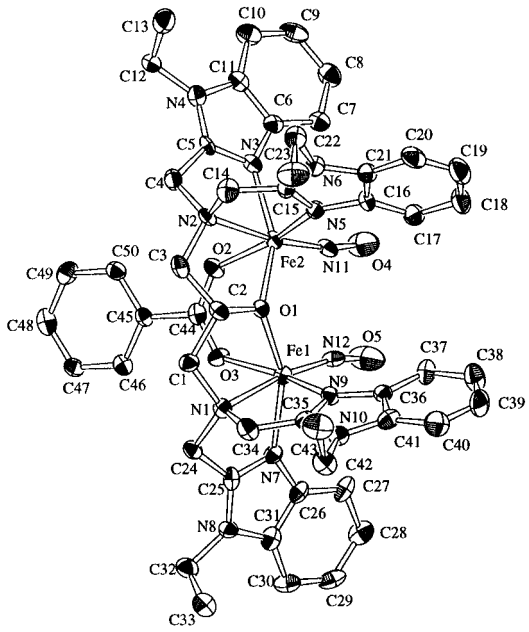

Figure 1. ORTEP representation of the cation of **1b** (40% probability ellipsoids) with hydrogen atoms removed for clarity.

octahedral geometry lie along the O(1)−Fe(2)−N(3) and O(1)−Fe(1)−N7 vectors. These angles are bent by 26.5° from the ideal 180° value and in a direction normal to the plane defined by the two $\{FeNO\}^7$ units such that O1 is displaced 0.455 Å from that plane.

The nitrosyl ligands on the different iron atoms are equivalent. Both species display the short Fe−N (Fe−N_{av} = 1.750(1) Å) and N−O (N−O_{av} = 1.154(4) Å) bond lengths typical of metal nitrosyl adducts and slight bend angles of 166.6(7)° and 168.3(7)° that are intermediate between the strictly linear and 120° extremes. Together, the two $\{FeNO\}^7$ units form an approximate plane with the nitrosyls bent slightly away from one another, a geometry that does not appear to be caused by steric factors. The Fe−N_{aliph} bonds are longer than the Fe−N_{arom} ones, a distinction consistent with general observations of metal−amine complexes.[23,35]

Optical and Vibrational Spectroscopy. The NO stretching frequency in compound **1b** occurs at 1785 cm^{-1}. Use of this value alone as an indicator of the Fe−NO binding mode is generally uninformative since the ranges for linear and bent complexes overlap significantly. The optical spectra of **1a**−**c** are shown in Figure 2. For **1a**, the visible region is featureless and consists only of a tail from a strong UV band. A broad feature centered at 620 nm ($\epsilon = 579 \pm 7$ M^{-1} cm^{-1}) is present for **1b**, and a second band appears as a shoulder at 520 nm ($\epsilon = 395 \pm 6$ M^{-1} cm^{-1}). A common feature in the visible region of the spectra of Fe−NO adducts at 420 nm does not appear to be present for this complex, but it is difficult to be sure because of the underlying tail from the UV band. This latter band has its λ_{max} at 330 nm ($\epsilon \approx 26\,000$ M^{-1} cm^{-1}). The optical spectrum of **1c** in methanol (data not shown) matches that reported previously.[25]

Magnetic Properties. Magnetic data are displayed in Figures 3a,b as χ vs T and μ_{eff} vs T plots, respectively. At high temperatures, the μ_{eff} vs T curve could approach 5.48 μ_B, which would be consistent with two independent $S = {}^3/_2$ centers having $g = 2.0$. An $S = {}^3/_2$ spin state is typical of iron nitrosyl complexes and can be formally achieved by the antiferromagnetic interaction of high-spin Fe(III) ($S = {}^5/_2$) with NO$^-$ ($S = 1$) or high-spin Fe(II) ($S = 2$) with neutral NO ($S = {}^1/_2$). The susceptibility relationships are derived from the general isotropic exchange Hamiltonian, $H = -2J\mathbf{S}_1 \cdot \mathbf{S}_2$, where $S_1 = S_2 = {}^3/_2$. A

(31) O'Connor, C. J. *Prog. Inorg. Chem.* **1982**, *29*, 203.
(32) Mealli, C.; Proserpio, D. M. *J. Chem. Educ.* **1990**, *67*, 399.
(33) Chen, Q.; Lynch, J. B.; Gomez-Romero, P.; Ben-Hussein, A.; Jameson, G. B.; O'Connor, C. J.; Que, L., Jr. *Inorg. Chem.* **1988**, *27*, 2673.
(34) Weiss, A.; Dick, S. *Z. Naturforsch.* **1994**, *49b*, 1051.
(35) Hayashi, Y.; Suzuki, M.; Uehara, A.; Mizutani, Y.; Kitagawa, T. *Chem. Lett.* **1992**, 91.
(36) Pessiki, P. J.; Khangulov, S. V.; Ho, D. M.; Dismukes, G. C. *J. Am. Chem. Soc.* **1994**, *116*, 891.

Table 2. Final Positional Parameters of Atoms in the $[Fe_2(Et\text{-}HPTB)(O_2CPh)(NO)_2]^{2+}$ Cation of **1b**·3MeCN[a]

atom	x	y	z	B_{eq} (Å^2)[b]
Fe(1)	0.31162(10)	0.08822(8)	0.78190(8)	2.11(3)
Fe(2)	0.30769(9)	0.27057(8)	0.60111(8)	2.08(3)
O(1)	0.2846(4)	0.1424(3)	0.6596(3)	1.9(1)
O(2)	0.4688(4)	0.2027(4)	0.5985(4)	2.5(1)
O(3)	0.4713(4)	0.0805(4)	0.7154(4)	2.5(1)
O(4)	0.2748(7)	0.3826(5)	0.7268(5)	6.6(2)
O(5)	0.2895(7)	0.2272(5)	0.8772(5)	6.7(3)
N(1)	0.3237(5)	−0.0442(5)	0.7384(4)	2.3(2)
N(2)	0.3256(5)	0.2133(4)	0.4810(4)	2.0(2)
N(3)	0.3639(5)	0.3715(4)	0.4927(4)	2.2(2)
N(4)	0.4351(5)	0.4153(5)	0.3503(5)	2.7(2)
N(5)	0.1526(5)	0.3171(5)	0.5767(4)	2.2(2)
N(6)	0.0448(5)	0.3397(5)	0.4887(4)	2.5(2)
N(7)	0.3658(5)	−0.0215(5)	0.8827(4)	2.2(2)
N(8)	0.4344(5)	−0.1705(5)	0.9305(4)	2.4(2)
N(9)	0.1555(5)	0.0686(5)	0.8284(4)	2.2(2)
N(10)	0.0408(6)	−0.0208(5)	0.8545(4)	2.5(2)
N(11)	0.2888(5)	0.3300(5)	0.6838(5)	2.5(2)
N(12)	0.2957(5)	0.1803(5)	0.8310(4)	2.5(2)
C(1)	0.3501(7)	−0.0168(6)	0.6414(5)	2.5(2)
C(2)	0.2966(7)	0.0819(6)	0.6045(6)	2.6(2)
C(3)	0.3549(7)	0.1116(6)	0.5118(6)	3.0(2)
C(4)	0.4098(7)	0.2495(6)	0.4112(6)	2.8(2)
C(5)	0.4023(6)	0.3465(5)	0.4163(6)	2.0(2)
C(6)	0.3717(6)	0.4631(6)	0.4771(6)	2.3(2)
C(7)	0.3454(7)	0.5241(6)	0.5329(5)	2.6(2)
C(8)	0.3615(8)	0.6128(7)	0.4957(7)	3.5(3)
C(9)	0.4059(8)	0.6394(6)	0.4048(7)	3.7(3)
C(10)	0.4337(7)	0.5807(7)	0.3496(6)	3.4(3)
C(11)	0.4158(6)	0.4912(6)	0.3874(6)	2.4(2)
C(12)	0.4799(7)	0.4137(6)	0.2573(6)	3.0(2)
C(13)	0.4038(8)	0.4647(7)	0.1999(6)	4.1(3)
C(14)	0.2256(7)	0.2442(6)	0.4475(6)	3.2(2)
C(15)	0.1410(7)	0.3016(6)	0.5037(6)	2.5(2)
C(16)	0.0564(7)	0.3691(6)	0.6107(6)	2.5(2)
C(17)	0.0203(7)	0.4039(6)	0.6863(6)	2.9(2)
C(18)	−0.0821(7)	0.4545(7)	0.7058(6)	3.8(3)
C(19)	−0.1481(8)	0.4712(7)	0.6465(7)	4.4(3)
C(20)	−0.1151(7)	0.4358(7)	0.5726(7)	3.6(3)
C(21)	−0.0119(6)	0.3844(6)	0.5560(6)	2.5(2)
C(22)	0.0061(7)	0.3376(6)	0.4132(6)	3.2(2)
C(23)	−0.0515(8)	0.2592(7)	0.4371(6)	4.7(3)
C(24)	0.4098(6)	−0.1161(6)	0.7731(5)	2.3(2)
C(25)	0.4025(6)	−0.1044(6)	0.8628(6)	2.5(2)
C(26)	0.3746(6)	−0.0354(6)	0.9698(6)	2.5(2)
C(27)	0.3494(7)	0.0261(7)	1.0246(6)	3.2(2)
C(28)	0.3665(8)	−0.0067(7)	1.1080(6)	3.5(3)
C(29)	0.4097(8)	−0.1008(7)	1.1364(6)	3.7(3)
C(30)	0.4360(7)	−0.1626(6)	1.0835(6)	3.4(3)
C(31)	0.4172(7)	−0.1277(7)	0.9991(6)	2.8(2)
C(32)	0.4816(7)	−0.2694(6)	0.9327(6)	3.3(2)
C(33)	0.4021(8)	−0.3284(7)	0.9786(6)	4.4(3)
C(34)	0.2245(7)	−0.0751(6)	0.7708(6)	3.0(2)
C(35)	0.1402(7)	−0.0082(6)	0.8182(5)	2.5(2)
C(36)	0.0584(7)	0.1124(6)	0.8726(5)	2.5(2)
C(37)	0.0266(7)	0.1951(7)	0.8997(6)	3.1(2)
C(38)	−0.0775(8)	0.2183(7)	0.9452(7)	4.2(3)
C(39)	−0.1468(8)	0.1621(8)	0.9624(7)	4.3(3)
C(40)	−0.1167(8)	0.0806(7)	0.9347(7)	4.2(3)
C(41)	−0.0135(7)	0.0558(7)	0.8905(6)	2.9(2)
C(42)	−0.0019(7)	−0.0976(6)	0.8549(6)	3.6(3)
C(43)	−0.0593(8)	−0.0755(7)	0.7822(7)	4.7(3)
C(44)	0.5116(7)	0.1271(6)	0.6436(6)	2.3(2)
C(45)	0.6286(6)	0.0888(5)	0.6057(5)	2.0(2)
C(46)	0.6837(7)	0.0088(6)	0.6508(5)	2.5(2)
C(47)	0.7883(7)	−0.0268(6)	0.6147(6)	2.7(2)
C(48)	0.8371(7)	0.0178(7)	0.5338(7)	3.3(3)
C(49)	0.7819(7)	0.0984(7)	0.4868(6)	3.1(2)
C(50)	0.6776(7)	0.1338(6)	0.5230(6)	2.5(2)

[a] Numbers in parentheses are errors in the last significant figure. See Figure 1 for atom-labeling scheme. [b] $B_{eq} = (4/3)[a^2\beta_{11} + b^2\beta_{22} + c^2\beta_{33} + 2ab\cos(\gamma)\beta_{12} + 2ac\cos(\beta)\beta_{13} + 2bc\cos(\alpha)\beta_{23}]$.

least-squares fit to the χ vs temperature curve required an additional term accounting for the presence of an impurity, assumed to be a mononuclear high-spin ferric species. The percentage of paramagnetic impurity was set at 1.4% and the g value was fixed at 2.0 during the final fitting procedure. Addition of a temperature independent paramagnetism term did not improve the quality of the fit and was omitted. The coupling constant J refined to a value of -23 cm^{-1}.

Table 3. Selected Bond Lengths (Å) for **1b**·3MeCN[a]

Fe(1)−O(1)	2.017(5)	Fe(2)−O(1)	2.006(5)
Fe(1)−O(3)	2.117(5)	Fe(2)−O(2)	2.134(6)
Fe(1)−N(1)	2.290(6)	Fe(2)−N(2)	2.282(7)
Fe(1)−N(7)	2.119(7)	Fe(2)−N(3)	2.114(7)
Fe(1)−N(9)	2.117(7)	Fe(2)−N(5)	2.135(7)
Fe(1)−N(12)	1.749(8)	Fe(2)−N(11)	1.750(7)
O(5)−N(12)	1.151(8)	O(4)−N(11)	1.156(8)

[a] Numbers in parentheses after distances are estimated standard deviations for the last significant digit. See Figure 1 for the atom-labeling scheme.

Table 4. Selected Bond Angles (deg) for **1b**·3MeCN[a]

Fe(1)−N(12)−O(5)	166.6(7)	Fe(2)−N(11)−O(4)	168.3(7)
O(1)−Fe(1)−O(3)	83.6(2)	O(1)−Fe(2)−O(2)	82.7(2)
O(1)−Fe(1)−N(1)	79.5(2)	O(1)−Fe(2)−N(2)	79.3(2)
O(1)−Fe(1)−N(7)	153.6(2)	O(1)−Fe(2)−N(3)	153.4(2)
O(1)−Fe(1)−N(9)	89.8(2)	O(1)−Fe(2)−N(5)	91.8(2)
O(1)−Fe(1)−N(12)	107.8(3)	O(1)−Fe(2)−N(11)	108.0(3)
O(3)−Fe(1)−N(1)	87.0(2)	O(2)−Fe(2)−N(2)	86.6(2)
O(3)−Fe(1)−N(7)	87.4(2)	O(2)−Fe(2)−N(3)	86.7(2)
O(3)−Fe(1)−N(9)	164.1(2)	O(2)−Fe(2)−N(5)	164.0(2)
O(3)−Fe(1)−N(12)	98.0(3)	O(2)−Fe(2)−N(11)	97.7(3)
N(1)−Fe(1)−N(7)	75.2(2)	N(2)−Fe(2)−N(3)	75.7(2)
N(1)−Fe(1)−N(9)	77.6(3)	N(2)−Fe(2)−N(5)	77.6(2)
N(1)−Fe(1)−N(12)	171.5(3)	N(2)−Fe(2)−N(11)	171.9(3)
N(7)−Fe(1)−N(9)	92.3(2)	N(3)−Fe(2)−N(5)	91.7(2)
N(7)−Fe(1)−N(12)	98.0(3)	N(3)−Fe(2)−N(11)	97.6(3)
N(9)−Fe(1)−N(12)	97.7(3)	N(5)−Fe(2)−N(11)	98.2(3)
Fe(1)−O(1)−Fe(2)	117.7(2)		

[a] Numbers in parentheses after angles are estimated standard deviations for the last significant digit. See Figure 1 for the atom-labeling scheme.

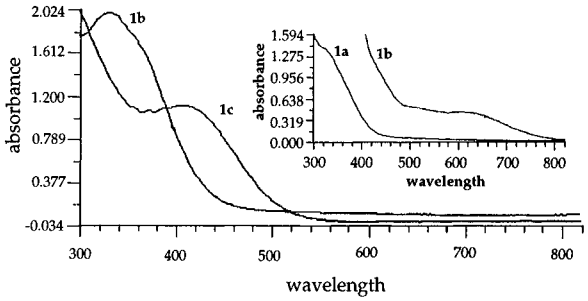

Figure 2. Optical spectra of **1a**−**c** in MeCN. The spectrum of **1b** was collected under 1 atm of NO. The inset shows the spectra of **1a**,**b** at a higher concentration so that the absorption bands in the visible region can be observed.

Mössbauer Properties. The 4.2 K Mössbauer spectrum of polycrystalline **1b** consists of a single quadrupole doublet (Figure 4). Least-squares fitting of the data yielded an isomer shift, δ, of 0.67 mm s^{-1} and a quadrupole splitting, ΔE_Q, with a magnitude of 1.44 mm s^{-1}.

Discussion

The dinitrosyl complex, $[Fe_2(Et\text{-}HPTB)(O_2CPh)(NO)_2](BF_4)_2$ (**1b**), offers an opportunity to gain insight into the bonding of diatomic ligands with a complex that models aspects of the active sites of non-heme diiron proteins. The synthesis of **1b** involves simple addition of NO to the diferrous complex, $[Fe_2(Et\text{-}HPTB)(O_2CPh)](BF_4)_2$, a reaction that mimics the NO binding ability of the reduced forms of hemerythrin and ribonucleotide reductase (R2). In hemerythrin, NO binds to only

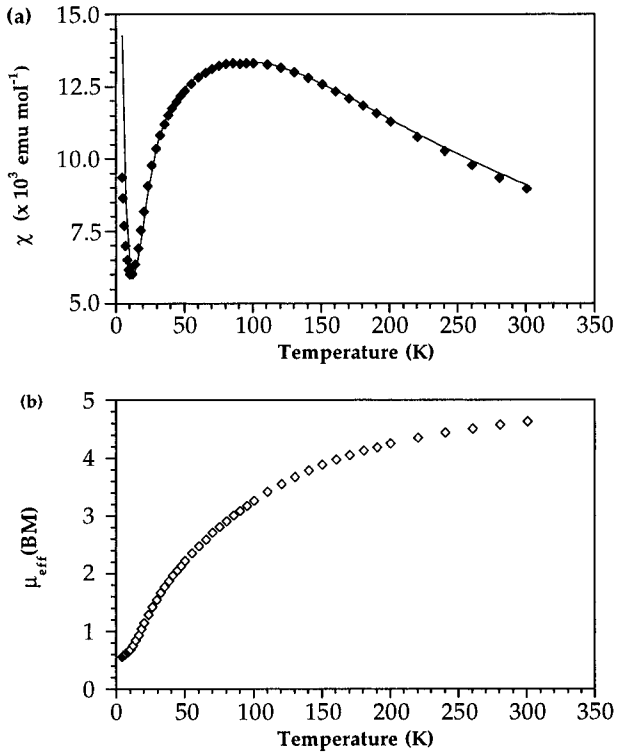

Figure 3. Magnetic susceptibility studies of **1b**. (a) Plot of χ versus temperature between 4.3 and 300 K. The solid line designates the fit to the model described in the text. (b) Plot of μ_{eff} versus temperature between 4.3 and 300 K.

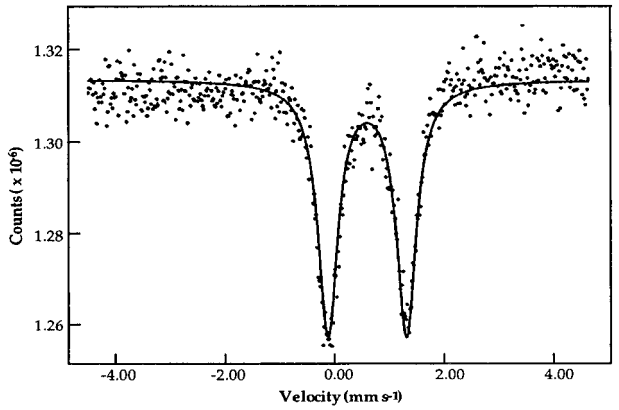

Figure 4. Solid-state Mössbauer spectrum of **1b** at 4.2 K. The solid line designates the least-squares fit using parameters described in the text.

one of the two iron atoms, the other being inaccessible to exogenous ligands. The resulting adduct is proposed to adopt a bent configuration analogous to the hydroperoxo ligand in oxyhemerythrin.[12] Although the geometry of the dioxygen, or peroxodiiron(III), adduct of R2 is unknown, each of the iron atoms of the reduced form, $R2_{red}$, can ligate nitric oxide, leading to a $\{FeNO\}_2$ species.[13] The ability to isolate **1b** is significant since the corresponding peroxo adduct, $[Fe_2(Et\text{-}HPTB)(O_2CPh)(O_2)](BF_4)_2$, is stable only at temperatures below −20 °C.[23,37]

The syn orientation of the two Fe−NO sites in **1b** resembles a transition state suggested for decomposition of the dinitrosyl adduct of ribonucleotide reductase.[13] Addition of NO to $R2_{red}$ initially produces a $\{FeNO\}_2$ complex, which decomposes upon standing to yield $R2_{met}$ and N_2O. It was proposed that coupling of the two nitrosyl ligands generates a transient N_2O_2 species containing an N−N bond. In this hypothetical reaction scheme, elimination of N_2O would allow the remaining oxygen atom to bridge the diferric centers in $R2_{met}$ (eq 2). It should be noted,

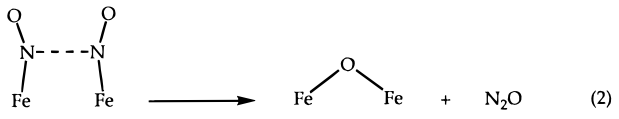

(2)

however, that the R2 dinitrosyl adduct is prepared with excess NO. Electrophilic attack of free NO on a single bound NO ligand can produce a $Fe-N_2O_2$ species,[2,38] which could conceivably rearrange to the Fe−O−Fe moiety with net elimination of NO and N_2O. Acetonitrile solutions of **1b**, however, are stable both in the presence and absence of NO over a period of 1 day at room temperature. Loss of the nitrosyl ligand appears to be a kinetically slow process; warming the sample to 40 °C facilitates nitrosyl dissociation to yield the diferrous starting material, $[Fe(Et\text{-}HPTB)(O_2CPh)](BF_4)_2$. The NO ligand also appears to dissociate in the solid state; the elemental analysis corresponds to a stoichiometry of only 1.2 nitrosyl ligands per formula unit.

Exposure of **1b** to dioxygen generates the bis(nitrato) complex, $[Fe_2(Et\text{-}HPTB)(NO_3)_2(OH)](BF_4)_2$ (**1c**). Reaction of bound nitrosyls with dioxygen can result in the formation of either nitrito or nitrato complexes, where the initial step is electrophilic attack of dioxygen on the nitrogen atom.[38] This intermediate could then react with another nitrosyl complex and undergo O−O bond cleavage to form a nitrito complex or could rearrange intramolecularly to generate the nitrato ligand (Scheme 1). Clearly the iron centers in **1b** act like independent units in which both peroxynitrite intermediates formally undergo separate intramolecular rearrangements. Performing the reaction under an excess of dioxygen, as was the case here, will decrease the probability of intermolecular pathways.

Scheme 1

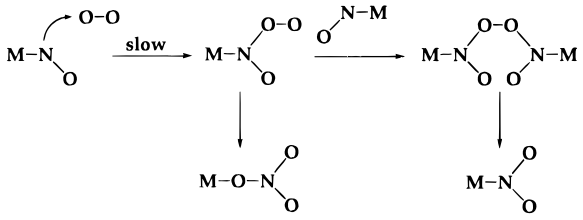

The physical properties of the $\{FeNO\}^7$ centers in **1b** are comparable to those of similar mononuclear non-heme iron complexes. The ν_{NO} value of 1785 cm^{-1} observed in the IR spectrum falls in the expected range for 18-electron octahedral complexes, after applying the correction for charge and considering the position of Fe in the periodic table.[39] The presence of only one NO stretch indicates the absence of significant vibrational coupling between the two $\{FeNO\}^7$ centers, which would produce symmetric and asymmetric stretching modes which are infrared active in a complex of C_s symmetry.

The δ and $|\Delta E_Q|$ values in the Mössbauer spectrum of **1b**, 0.67 and 1.44 mm s^{-1}, respectively, are consistent with those of other non-heme $\{FeNO\}^7$ complexes and protein active sites (Table 5). The use of Mössbauer parameters as a means to assign formal oxidation states to metal centers can be risky. X-ray absorption pre-edge and rising edge data are more reliable measures of the metal oxidation state. Such data were used to assign the iron atom in [Fe(edta)(NO)] as ferric, together with force constant and charge transfer spectroscopic information.[11]

(37) Feig, A. L.; Becker, M.; Schindler, S.; van Eldik, R.; Lippard, S. J. *Inorg. Chem.* **1996**, *35*, 2590.

(38) Bottomley, F. In *Reactions of Coordinated Ligands*; Plenum Press: New York, 1989; Vol. 2, p 115.

(39) Haymore, B. L.; Ibers, J. A. *Inorg. Chem.* **1975**, *14*, 3060.

Table 5. Mössbauer Parameters for {FeNO}^{7} Systems

{FeNO}^{7} host	δ (mm s^{-1})	ΔE_Q (mm s^{-1})	ref
protocatechuate 4,5-dioxygenase/substrate	0.66	−1.67	3
[Fe^{II}(edta)]	0.66	−1.67	3
1a[a]	0.67	1.44[b]	this work
deoxyhemerythrin	0.68	0.61	12
putidamonooxin/substrate	0.68	−1.4	4
[Fe^{II}(5-Cl-salen)]	0.69	0.57	8
ribonucleotide reductase	0.70	−1.7	13
isopenicillin N synthase	0.75	−1.0	7

[a] $[Fe_2(Et\text{-}HPTB)(O_2CPh)]^{2+}$. [b] Magnitude only; sign was not determined.

The fact that the Mössbauer parameters of [Fe(edta)(NO)] are very similar to those of **1b** may indicate that iron in the latter should also be assigned a +3 formal oxidation state, but such an assignment is equivocal in the absence of XAS or other more definitive data.

An investigation of the temperature-dependent magnetic susceptibility properties of solid **1b** revealed substantial internal coupling of the two high-spin iron centers and two odd-electron ligands. The magnetic interactions of these units can be formally delineated by assigning $S = {}^3/_2$ spin states to the {FeNO}^{7} centers, as indicated above. The resulting two $S = {}^3/_2$ centers then experience a weak antiferromagnetic exchange coupling. The derived coupling constant, J, of -23 cm^{-1} is in the range previously reported for non-heme (μ-alkoxo)- and (μ-hydroxo)diiron(III) complexes.[40]

For compounds containing mononuclear {FeNO}^{7} centers, two theoretical approaches have been used to explain the commonly observed $S = {}^3/_2$ ground state, namely, extended Hückel calculations, as applied for example to $[Fe(H_2O)_5(NO)]^{2+}$,[9] and an SCF-Xα analysis, which separates the metal and ligand orbital fragments. The results of the latter kind of study showed that a model in which high-spin Fe(III) ($S = {}^5/_2$) is antiferromagnetically coupled to NO$^-$ ($S = 1$) correlates well with experimental determinations.[10,11]

The singly occupied highest molecular orbital (HOMO) of many octahedral {FeNO}^{7} complexes has substantial Fe−N π antibonding character involving the metal d and NO π^* orbitals.[14] Owing to the distorted octahedral geometry of **1b**, especially the nonlinear *trans*-(μ-alkoxo)−Fe−N axis (Figure 1), we carried out an extended Hückel study[41] to investigate the nature of the Fe−NO bonds. The theoretical complex $[Fe_2(NO)_2(NH_3)_6(O_2CH)(OH)]^{2+}$ was used to model **1b**. The Walsh diagram for this diiron model, depicted in Figure 5, displays the energy levels as a function of varying the Fe−N−O angle from 120 to 180° in 10° increments while maintaining C_s symmetry. Only the levels with significant metal d orbital character are depicted. The solid vertical line in the figure demarcates the experimentally observed 167° Fe−N−O angles in **1b**. We shall discuss the results for a 170° Fe−N−O angle, since it closely resembles the situation for **1b** and has a set of energy levels quite similar to those for the 180° Fe−N−O case. The major consequence of distorting the *trans*-(μ-alkoxo)−Fe−N angles from linearity is stabilization of the $d_{x^2-y^2}$ orbitals through mixing with the d_{xy} orbitals in energy levels labeled 25a″, 28a′, 28a″, and 31a′ in the diagram.

The HOMO, 29a′, has considerable Fe d_{xz}/N p_x π-antibonding character. If the energy of this level alone controlled the preferred geometry, as it does with many transition metal nitrosyl complexes, a 120° Fe−NO angle would be expected, according to the Walsh diagram. As can be seen, bending the Fe−N−O angle diminishes the antibonding interaction (Figure 6, 29a′ −120° and 29a′ −170°). In **1b**, however, the observed Fe−N−O bend is also affected by two other orbitals, 24a″ and 27a′, in which π-bonding occurs between the Fe d_{xz} and NO π^* orbitals. As the Fe−N−O angle decreases from 170 to 120°, so too do these favorable Fe−N π interactions, as illustrated in Figure 6 (24a″ −120° and 24a″ −170°). The significance of Fe−N π bonding is further emphasized by the Fe d_{xz}−N p_x overlap populations. For both the 120 and 170° situations, this value is positive, indicating an overall bonding interaction. As the Fe−N−O angle is increased from 120° to 170°, the overlap population experiences a 3-fold increase, from 0.03 to 0.097. Thus the Fe−N π bonding is more significant at larger Fe−N−O angles and dominates the interaction. Bending the Fe−N−O angle results in more σ-type interaction between iron and nitrogen in 24a″ because there is mixing of the d_{z^2} orbital with the d_{xz} orbital. No additional contributions arise from iron p orbitals, however, that would further strengthen the Fe−N bond in the bent configuration. There is an appreciable amount of iron d and nitrogen p orbital character in the 27a′, 24a″, and

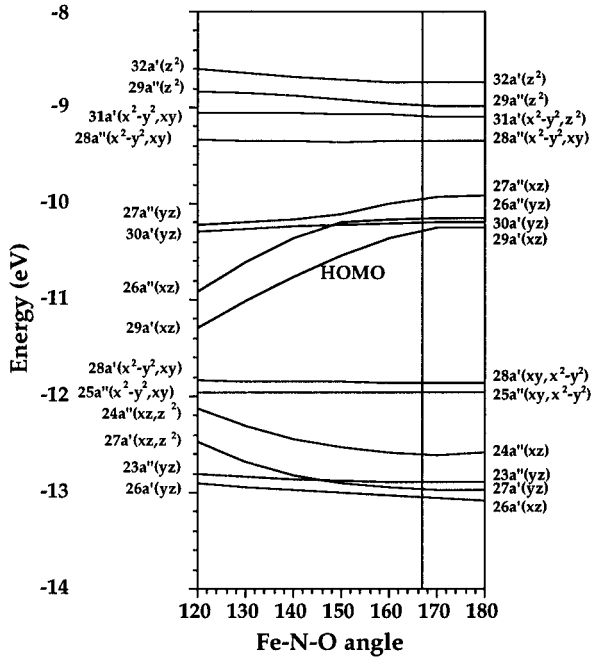

Figure 5. Walsh diagram for the complex $[Fe_2(NO)_2(NH_3)_6(O_2CH)(OH)]^{2+}$, which models **1b**. The Fe−N−O angle is increased by 10° increments from 120 to 180°, maintaining C_s symmetry.

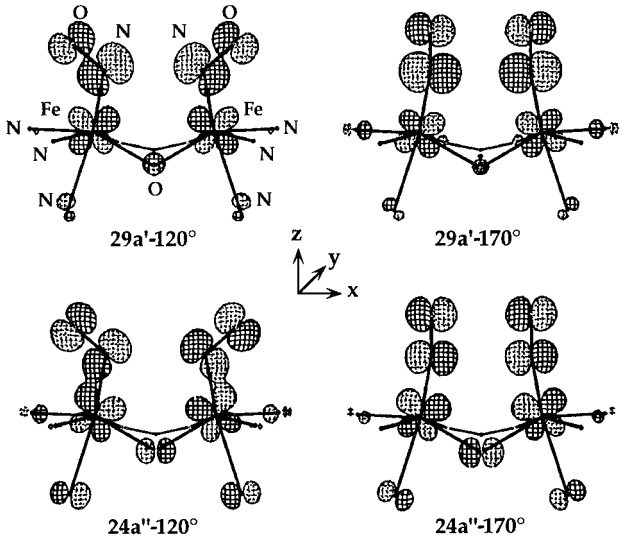

Figure 6. Molecular orbitals for the 29a′ and 24a″ levels looking down the *y*-axis, where the Fe−N−O angle is 120° and 170°.

(40) Kurtz, D. M. *Chem. Rev.* **1990**, *90*, 585.
(41) Hoffmann, R. *J. Chem. Phys.* **1963**, *39*, 1397.

Table 6. Percent Character of Fe d and Nitrosyl N and O p Orbitals in the Model Complex $[Fe_2(NO)_2(NH_3)_6(O_2CH)(OH)]^{2+}$ with an Fe−N−O Angle of 170°

orbital	% d character (per Fe)	% p character (per N)	% p character (per O)
27a′	27	7	11
24a″	25	9	11
29a′	17	22	8

29a′ orbitals, indicating substantial covalent bonding between iron and the nitrosyl ligand in **1b** (Table 6).

Nitric oxide is capable of acting as an oxo- or NO-transfer agent.[15,38] To determine whether **1b** could effect such chemistry, olefins were added to the complex under a variety of conditions. Although no oxo-transfer reactions occurred, we did observe catalytic olefin nitration by a catalyst formed upon addition of excess nitric oxide to the preformed peroxo complex, $[Fe_2(Et\text{-}HPTB)(O_2CPh)(O_2)](BF_4)_2$, in the strict absence of excess dioxygen.[42] Controls showed that olefin nitration did not occur in the absence of catalyst in nitrile solvent. The synthetic utility of this chemistry is diminished, however, by a recent report that olefin nitration can be effected by the simple addition of NO in an appropriate solvent.[43]

Summary and Conclusions

The dinitrosyl diiron complex **1b** was isolated from the reaction of NO with the diiron(II) compound **1a**. An X-ray crystallographic study revealed that the FeNO units are equivalent, having distorted octahedral geometry and displaying only moderate Fe−N−O bend angles. The two $S = {}^3/_2$ $\{FeNO\}^7$ moieties are antiferromagnetically coupled, with an exchange coupling constant of -23 cm^{-1}, where $H = -2J\mathbf{S}_1\cdot\mathbf{S}_2$. Upon exposure to dioxygen, the complex oxidizes to form a bis(nitrato) complex, **1c**, consuming 2 equiv of dioxygen. The Mössbauer parameters are comparable to those of other chemical and biological $\{FeNO\}^7$ centers. An extended Hückel study on the **1b** model complex, $[Fe_2(NO)_2(NH_3)_6(OH)(O_2CH)]^{2+}$, indicates that the 167° Fe−N−O bond angle is determined by the Fe−N π bonding orbitals and not by the HOMO, which is Fe−N π antibonding.

Acknowledgment. This work was supported by grants from the National Institute for General Medical Science and AKZO Corp. We thank Drs. G. C. Papaefthymiou for collecting and fitting the Mössbauer data and M. J. Scott for assistance with the crystallographic data collection.

Supporting Information Available: Tables S1−S4, reporting positional and thermal parameters, bond lengths, bond angles, and anisotropic thermal parameters for all atoms in **1b** (12 pages). Ordering information is given on any current masthead page.

IC960552B

(42) Feig, A. L. Ph.D. Thesis, Massachusetts Institute of Technology, 1995.
(43) Hata, E.; Yamada, T.; Mukaiyama, T. *Bull. Chem. Soc. Jpn.* **1995**, *68*, 3629.
(44) Carnahan, E. M.; Rardin, R. L.; Bott, S. G.; Lippard, S. J. *Inorg. Chem.* **1992**, *31*, 5193.